ELSEVIER

Ceramics International 31 (2005) 851–862

CERAMICS INTERNATIONAL

www.elsevier.com/locate/ceramint

Microstructure and mechanical properties of ultrafine Ti(CN)-based cermets fabricated from nano/submicron starting powders

Sheng Chao[a], Ning Liu[a,*], Yupeng Yuan[a], Chengliang Han[a], Yudong Xu[a], Min Shi[a], Jianping Feng[b]

[a]*Department of Materials Science and Engineering, Hefei University of Technology, Hefei 230009, PR China*
[b]*Department of Mechanics, University of Science and Technology of China, Hefei 230026, PR China*

Received 30 April 2004; received in revised form 5 May 2004; accepted 15 September 2004
Available online 13 January 2005

Abstract

Starting from commercial nano/submicron raw powders, ultrafine grade (mean grain size less than 500 nm) titanium carbonitride (Ti(CN))–WC–Mo–Ni/Ni + Co–C cermets systems were fabricated and their microstructures as well as mechanical properties were characterized, tested and compared with coarse (micron-sized) cermets. Study shows that different raw materials and initial powder particle size play a critical role in determining cermets' microstructure and mechanical properties. X-ray diffractometry (XRD) and scanning electron microscopy (SEM) in combination with energy dispersive X-ray analysis (EDX) reveal that various cermets systems present quite different morphological and structural characteristics. The reasons why these differences come about were discussed and the formation mechanism of a new type core/rim structure (white core and grey rim) was proposed too. Mechanical property testing was conducted and was related to the microstructural features.

Keywords: B. Microstructure-final; C. Mechanical properties; D. Carbides; D. Nitrides

1. Introduction

Titanium carbonitride-based (Ti(CN)-based) cermets are important structural and wear-resistant materials which are widely appreciated in metal cutting application, owing to their excellent mechanical properties [1–3]. Recently, more and more conventional WC–Co-based hard metals are being replaced by Ti(CN)-based cermets, accompanied with the trend of high speed machining. Comparing with WC–Co hard metal, the advantages of Ti(CN)-based cermets lie in their higher hot hardness, wear resistance, chemical stability, and resistance to plastic deformation at elevated temperature. Consequently, cermets cutting tools show improved surface finishing and tolerance control. Meanwhile, the cutting efficiency and tool life are improved too. On the whole, in high speed finishing and semi-finishing cutting applications, Ti(CN)-based cermets are more preferred than WC–Co hard metals [4–6].

The complex microstructure of Ti(CN)-based cermets is the key to interpret their mechanical properties, so it has been widely studied by many authors for years [7–9]. Generally, cermets material is composed of two phases: one is the ceramic phase (titanium carbonitride hard phase) and the other is metal binder phase (nickel or cobalt or a mixture of them) that bonds the ceramic phase. In general, ceramic phase provides high hardness to this class of materials, while the metal binder phase contributes to ductility, toughness and thermal-shock resistance. Microstructural examination shows that a typical carbonitride grain often demonstrates a core/rim structure: black Ti(CN) cores surrounded by grey (Ti, W, Mo, Nb, Ta, ...) (C, N) complex carbonitride rims (in scanning electron microscopy (SEM)–back-scattered-electron (BSE) contrast), resulting from a dissolution–reprecipitation process.

Previous work has shown that by using nano-sized starting powders, the mechanical property (especially hardness) of

* Corresponding author. Tel./fax: +86 551 290 5383.
E-mail address: ningliu@mail.hf.ah.cn (N. Liu).

0272-8842/$30.00
doi:10.1016/j.ceramint.2004.09.013

Table 1
Main characteristics of the starting powders

Powder	ssa (m^2/g)	Particle size (μm)	Chemical composition (wt%)
TiC (fine)	12	0.33[a]	$C_{free} < 0.5$, Cl < 0.25, O < 1.0
TiC (coarse)	–	2–4[a]	C_{free}, 0.179; O, 0.13
TiN	27	0.07[a]	C < 1.0, O < 2.0
$Ti(C_{0.5}N_{0.5})$	23	0.12[a]	$C_{free} < 0.5$, Cl < 0.25, O < 1.0
WC	–	1.14 (Fsss)	C_{free}, 0.02
Mo	–	2.33 (Fsss)	C, 0.0036; Fe, 0.002; O, 0.095
Ni	–	2.95 (Fsss)	C < 0.15, S < 0.001, O < 0.015, Fe < 0.01
Co	–	2.46 (Fsss)	C, 0.058; S, 0.0045; O, 0.008
Carbon black	–	3.25 (Fsss)	N, 0.00015; O, 0.3

ssa, Specific surface area, Fsss, Fisher sub-sive size.
[a] From SEM/TEM analysis, other values come from datasheets of the producers.

WC–Co hard metals can be greatly enhanced [10]. Moreover, it was reported that nano-sized TiN addition is more effective than micron-sized TiN addition in improving the mechanical properties and the cutting performance of TiC-based cermets [11]. However, hitherto, there are few reports on the study of ultrafine grade Ti(CN)-based cermets. Our purpose in this work is to investigate the microstructure and mechanical properties of Ti(CN)-based cermets fabricated from nano/submicron-sized powders and compare them with micron-sized cermets. In this present work, Ti(CN) was introduced from two different ways: TiC + TiN or $Ti(C_{0.5}N_{0.5})$ (abbreviated as Ti(CN) afterwards). In addition, the effect of different molybdenum addition and the influence of Ni + Co mixed binder composition were also studied.

2. Experimental procedure

2.1. Specimen preparation

The characteristics of commercially obtained starting powders are listed in Table 1. Fig. 1a–d are the SEM images of hard phase powders, which show cubic-shaped TiC (fine) and Ti(CN) powders, spherical-shaped TiN powders and irregular-shaped TiC (coarse) powders. After weighing and ultrasonic dispersion, raw powders were milled in a planetary ball mill. Blending was done at 200 rpm with WC–Co balls (ball-to-powder weight ratio, 8:1) for 36 h in ethanol bath. Then, the slurry mixture was dried for 12 h at the temperature of 80 °C, after which dried powders were sieved through No. 200 mesh and pelletised. Rectangular-shaped specimens were pressed at uniaxial pressure of 200 MPa for transverse rupture strength (TRS) and fracture toughness (K_{IC}) test. Finally, green specimens were dewaxed at 800 °C, and vacuum sintered (0.1 Pa) at 1440 °C for an hour. A series of four model systems were prepared by exactly the same method, and their nominal compositions are given in Table 2.

2.2. Experimental methods

The microstructure of polished specimens (finished with 1 μm diamond paste) was observed by SEM (LEO-1530VP, LEO, Germany) in BSE mode coupled with EDX, (OXFORD INCA X-Sight, UK), and the fractured surface was observed in the secondary electron (SE) mode. Only metallic constituents of each sample were measured in this study since carbon and nitrogen content cannot be accurately quantified from SEM–EDX. Semi-quantitative information about grain size and phase volume fraction was obtained by manual measurements on SEM micrographs using standard linear intercept and point counting methods, respectively. Phase identification of each system was carried out by XRD (D/max-rB, Rigaku, Japan) and the lattice parameter of crystalline phase was calculated by using Nelson–Riley function [12] (Ni-filtered Cu Kα radiation, $85^\circ < 2\theta < 145^\circ$ angular range, 0.02° angle step). Three-point-bending TRS (20 mm span, 0.5 mm/min crosshead speed) and K_{IC} (single edge notched beam (SENB) method) testing was carried out on a Shimadzu DCS-5000 Universal Testing Machine (Japan) at room temperature. The specimen geometric sizes are 5 mm × 5 mm × 30 mm and 2.5 mm × 5 mm × 30 mm for TRS and K_{IC} testing, respectively. To specimen used for K_{IC} testing, a pre-made sharp crack was introduced in the middle of the length. Vickers indentation hardness with a load of 10 kg, 15 s loading time was measured and the density of each specimen is calculated by using Archimedes method.

3. Results and discussion

3.1. Microstructure and phase composition

Fig. 2 illustrates the representative microstructures of four sample systems, from which it can be seen that all samples contain black cores and grey rims in SEM–BSE contrast. SEM–EDX analysis reveals that the metallic constitutes of black core are mainly titanium with little molybdenum and tungsten, because little amount of molybdenum and tungsten atoms can diffuse through dislocations and other crystal defects into Ti(CN) cores [13]. Actually these black Ti(CN) cores are remnants of Ti(CN) raw powders (for cermet C and cermet D) or TiC powders (for cermet A and cermet B) that have been nitrided

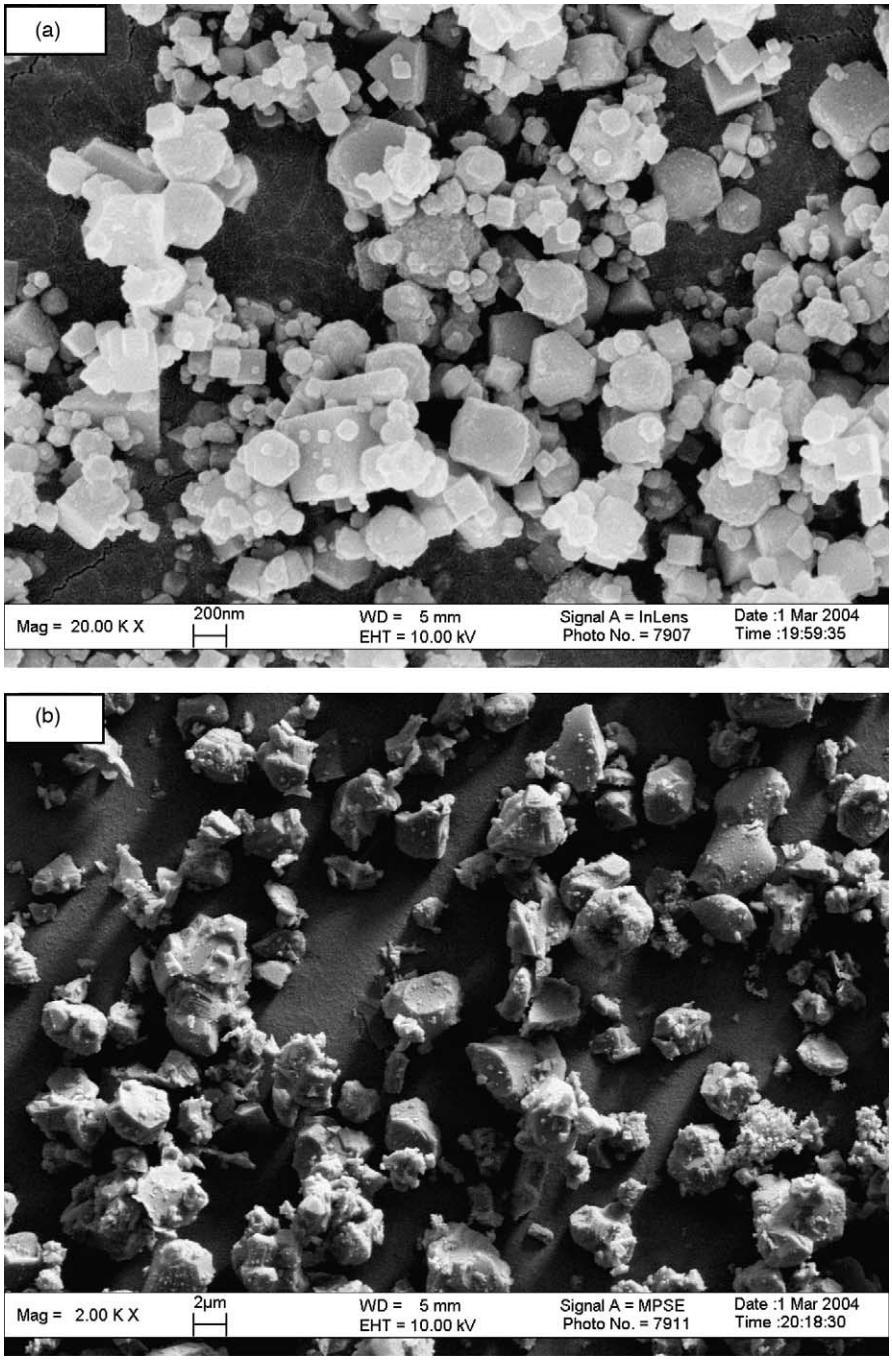

Fig. 1. SEM images of starting powders: (a) TiC (fine), (b) TiC (coarse), (c) TiN and (d) Ti(CN).

during sintering [14]. Much more molybdenum and tungsten contents were found in grey rims, and the inner rim located at the interface of the core and the outer rim (see Fig. 2b) existing in cermet B was even more W, Mo-rich than its outer rims. The metallic constitutes in each phase of four sample systems are given in Tables 3 and 4. Besides these common microstructural features, these four model systems demonstrate apparently different morphologies in terms of grain size, grain-size distribution, phase volume fraction, phase composition, and agglomeration status. Some of their microstructural parameters are summarized in Table 5.

Table 2
Nominal composition of cermets samples (in wt%)

Specimen	Ti(CN)	TiC	TiN	WC	Mo	Ni	Co	C
A	–	39 (fine)	10	15	15	20	–	1
B	–	39 (coarse)	10	15	15	20	–	1
C	49	–	–	15	15	20	–	1
D	59			15	5	10	10	1

Both cermet A and cermet B exhibit typical Ti(CN)-based cermets microstructures: ceramic phase with core/rim structure embedded in the metal binder. However, detailed

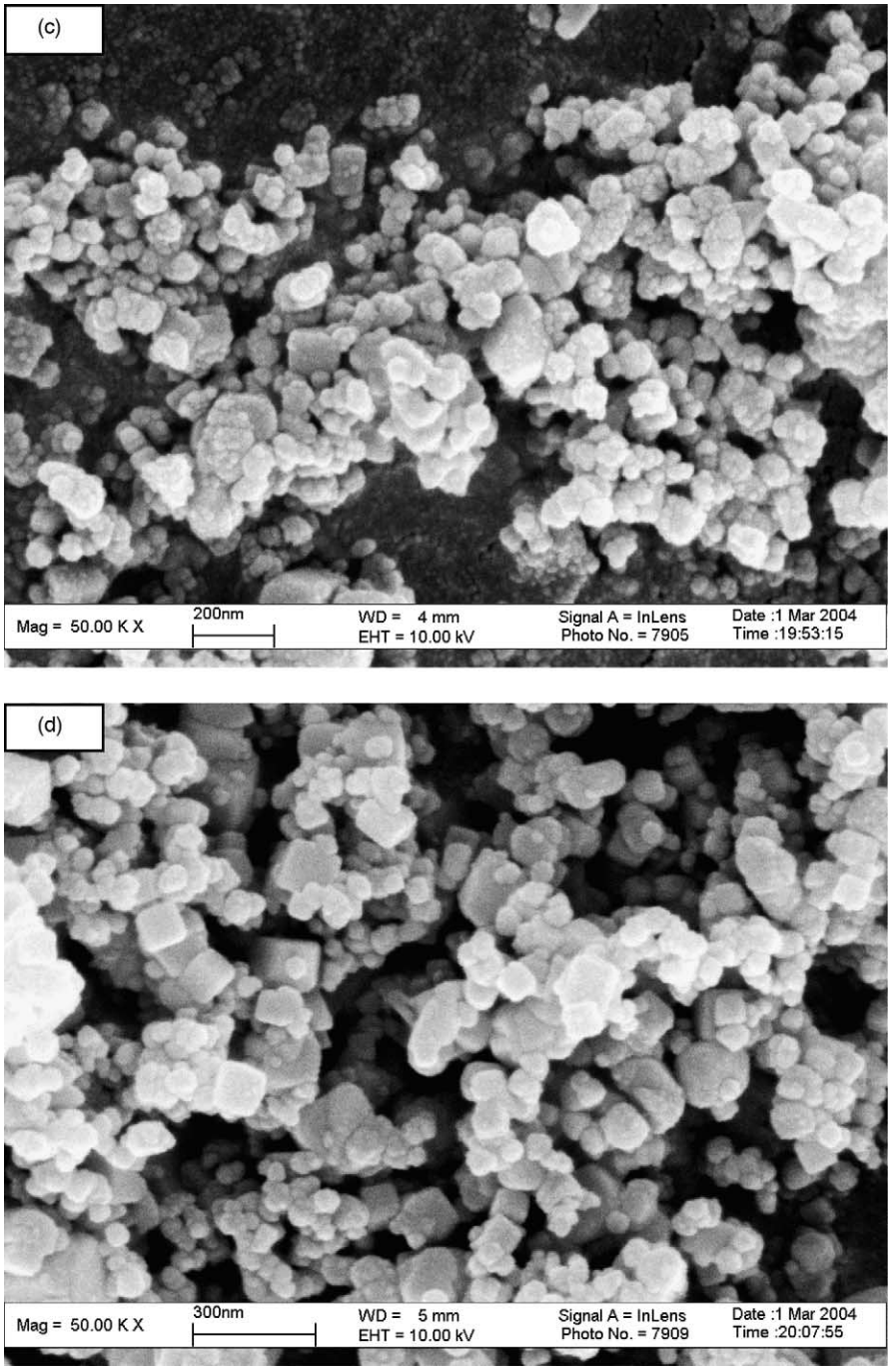

Fig. 1. (*Continued*).

examination revealed their differences. Comparing Fig. 2a with b, it is evident that: (1) The outer rim thickness of cermet A is much thinner than that of cermet B. (2) The core size of cermet B is smaller than its initial TiC particle size while the core size of cermet A almost preserved its initial TiC particle size. (3) Inner rim structure was not present in cermet A. Since the outer rim is formed during liquid phase sintering through a dissolution and reprecipitation process [13,15], thicker outer rim and smaller remaining Ti(CN) cores mean that coarser TiC powders have a larger solubility in liquid binder phase. That is to say more coarse TiC particles dissolved in liquid binder and together with dissolved WC and Mo_2C (Mo_2C was formed from the reaction of molybdenum and carbon during sintering below the temperature of 1000 °C, and then completely dissolved at 1200 °C according to literature [15]) precipitated on remaining TiC particles as rim phase. Considering that smaller particle size leads to higher surface energy, this phenomenon is in agreement with the general principle that the higher the surface energy of a substance is, the lower

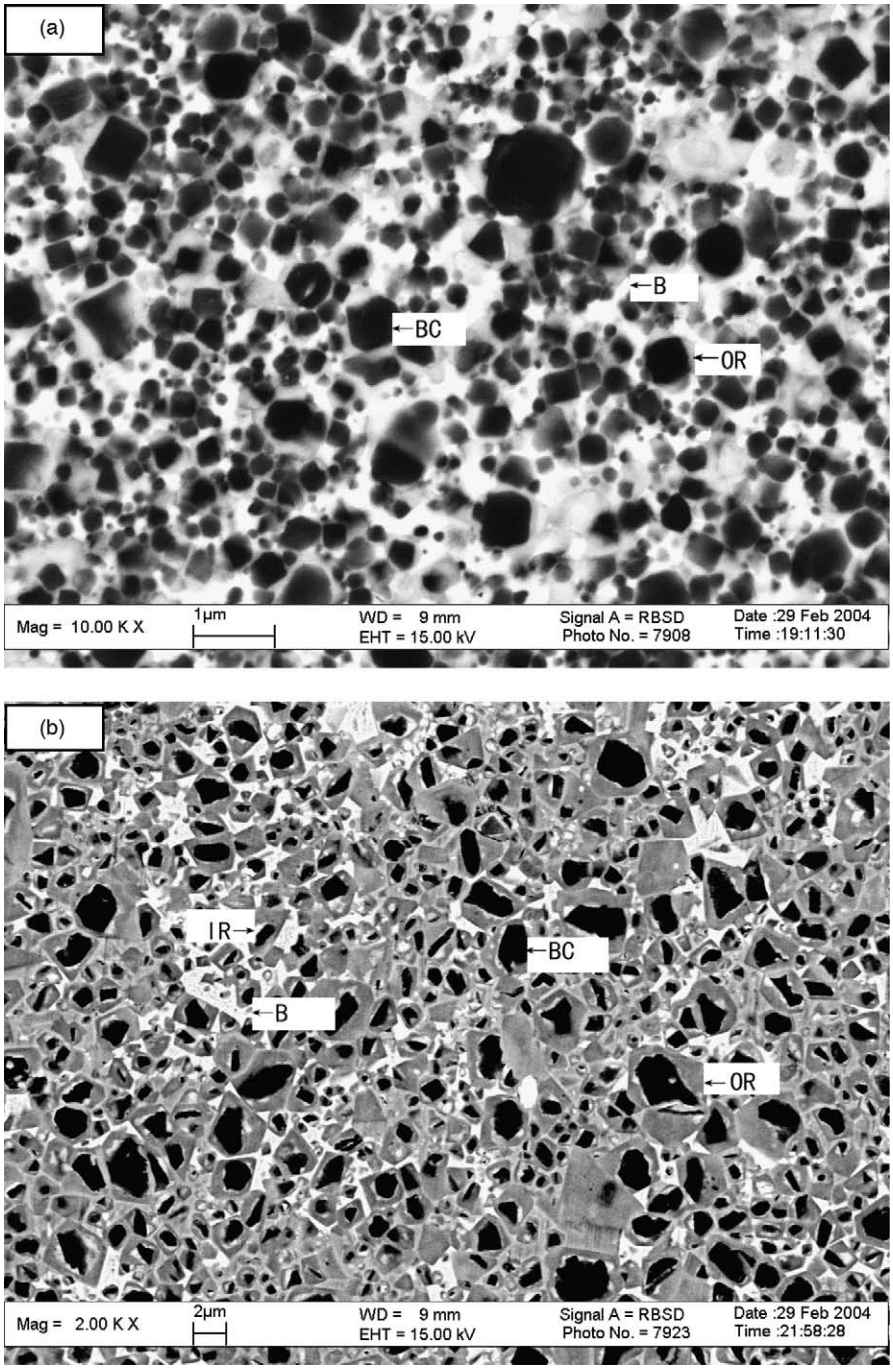

Fig. 2. SEM (BSE) micrographs of cermets (a) A, (b) B, (c) C and (d) D. BC, black core (Ti(CN) core); WC, white core ((Ti, W, Mo) (CN) core); IR, inner rim; OR, outer rim; B, binder.

solubility it has in a molten metal [16]. Additionally, the well-developed rim phases in cermet B may also result from more widespread coarse TiC particle size range, which promotes the process of dissolution and reprecipitation by Ostwald ripening mechanism.

The disappearance of inner rim in cermet A is an interesting phenomenon. Take into consideration that inner rim is formed during solid state sintering stage [7,8], and according to literature [9], the maximum solubility of tungsten in (Ti, W) C rim phase increases as increasing temperature (assuming that this finding can be extended to molybdenum too), the disappearance of inner rim may be explained by the following reason: higher activity of small TiC powders used in cermet A provides additional driving force for sintering, as a result, liquid phase forms at a relatively lower temperature as compared with cermet B. Therefore, solid state sintering is prematurely stopped (carried out at a lower temperature range), leading to lower

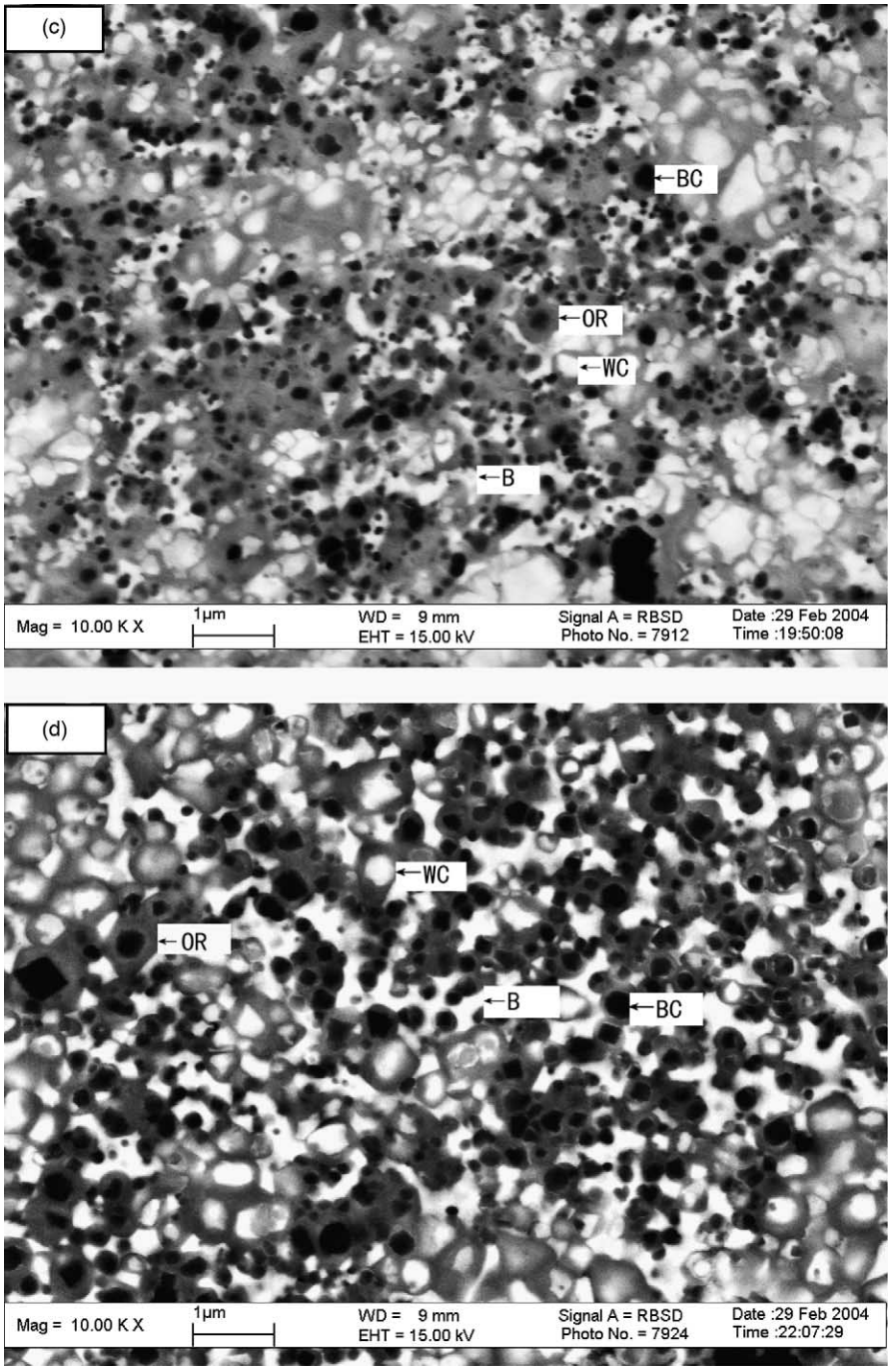

Fig. 2. (*Continued*).

diffusion rate of WC and Mo_2C and the formation of inner rim is repressed as a result.

The XRD profiles of four model systems are shown in Fig. 3, and the peak position, lattice parameter of Ti(CN) is listed in Table 6. Although the nominal composition of cermet A and cermet B is exactly the same, their XRD profiles show strikingly different patterns. In addition to normally observed Ti(CN) and nickel peaks, peaks of Ni_2W_4C exist in cermet A too. In some binder-shaped areas of cermet A, unusual high amount of tungsten (Ni/W ≈ 1/1, atomic ratio) was detected by SEM–EDX analysis, which further confirms the existence of this η phase. And its binder-shaped morphology indicates that it was formed during the cooling stage. Since the only difference between cermet A and cermet B is their initial powder particle size, the formation of Ni_2W_4C should be related to finer TiC powders used in cermet A. η phase is present in WC–Co hard metal and cermets in condition of carbon deficiency [17], so there is good reason to say that because of the high specific surface area of finer TiC initial powders used in cermet A, they

Table 3
Different carbonitride phases and their metallic constitutes (in at%)

Phase	Existing in	Ti	W	Mo
Ti(CN) core	A	94.2	2.7	3.1
	B	97.0	1.0	2.0
	C	91.7	4.9	3.4
	D	93.3	4.3	2.4
Inner rim	A	65.8	12.8	21.4
Outer rim	A	69.9	11.3	18.8
	B	75.8	10.6	13.6
	C	66.4	11.8	21.8
	D	85.0	10.9	4.1
(Ti, W, Mo) (C, N) core	C	61.5	13.8	24.7
	D	78.5	13.6	7.9

Table 4
Metallic constitutes (in at%) and lattice parameters of each binder phase

Specimen	Ti	W	Mo	Ni	Co	Lattice parameter (nm)
A	24.0	5.5	10.2	60.3		0.3602
B	19.7	5.3	9.8	65.2		0.3574
C	34.4	5.8	11.6	48.2		0.3613
D	38.5	5.0	4.0	29.0	23.5	0.3560
					Standard Ni	0.3524

contain much more oxygen contaminates (physically and chemically absorbed) than coarse TiC powders. So during sintering, large amount of carbon was consumed when it reacted with oxygen to form carbon monoxide and/or carbon dioxide (vacuum sintering condition promotes these reactions), which finally leads to carbon deficiency. In light of the fact that the formation of Ni_2W_4C consumes WC, less WC would be available to reprecipitate from the binder onto Ti(CN) cores. This reason together with previous-mentioned low solubility of fine TiC particles, prematurely stopped solid state sintering can be used to explain the nonexistence of inner rim and unusual thin outer rim found in cermet A.

Table 5
Some microstructural parameters of each sample system

Specimen	Mean core size (μm)	Mean grain size (core + rim) (μm)	Core phase	Rim phase (vol%)	Binder phase
A	0.29	0.35	44	40	16
B	1.38	2.47	23	62	15
C (black)	0.18	–	18	58	–
D (black)	0.22	0.28	21	55	14
D (white)	0.32	0.46	10	55	14

Another noticeable difference found in Fig. 3 is that all peaks of Ti(CN) in cermet B shift to the lower 2θ angles when compared with cermet A (see Table 6). This phenomenon indicates that the lattice parameter of Ti(CN) in cermet B is larger than that of cermet A. Considering that the dominant phase (phase of larger volume fraction) in cermet B is its rim phase while the dominant phase in cermet A is its core phase, so to be exact, those peaks represent (Ti, W, Mo) (C, N) rims and Ti(CN) cores for cermet B and cermet A, respectively. This phenomenon is consistent with the fact that the entrance of W and Mo atoms into the Ti(CN) sublattice expands the lattice parameter because the ionic

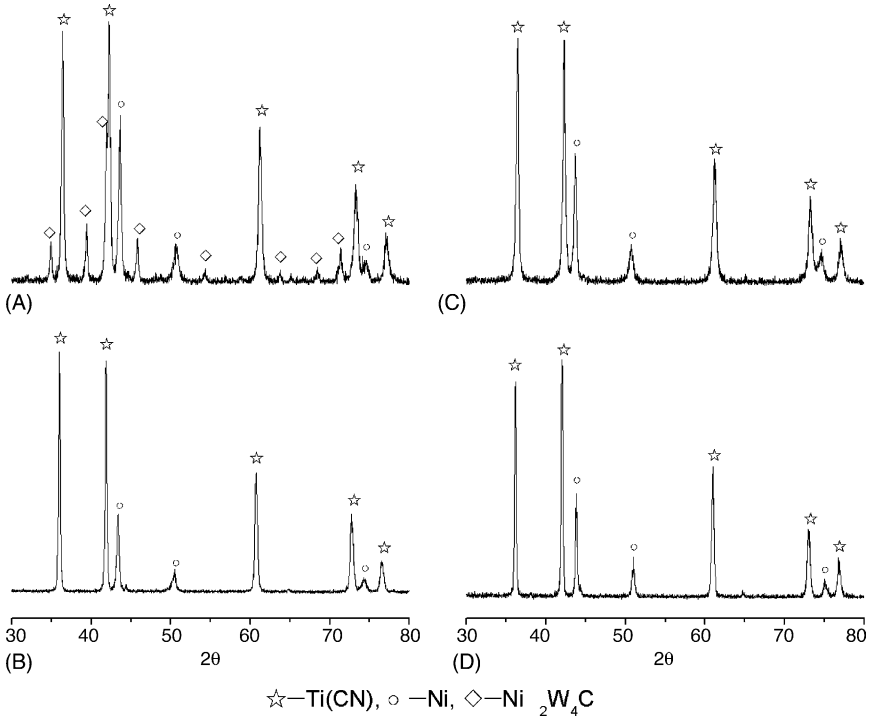

Fig. 3. XRD profiles of four model systems.

Table 6
Peak position and lattice parameter of Ti(CN)

Specimen	2θ Ti(CN)					Lattice parameter (nm)
	1 1 1	2 0 0	2 2 0	3 1 1	2 2 2	
A	36.42	42.26	61.22	73.26	77.20	0.4293
B	36.02	41.86	60.72	72.70	76.44	0.4306
C	36.42	42.28	61.20	73.20	77.10	0.4292
D	36.18	42.02	60.94	73.00	76.78	0.4296
Standard TiC						0.4327
Standard Ti(CN)						0.4290
Standard TiN						0.4242

radius of Ti^{4+} is 0.68 Å which is smaller than W^{4+} 0.70 Å and Mo^{4+} 0.70 Å.

There is no TiN, WC and Mo_2C peaks left in the XRD profiles after sintering, indicating that all these starting powders have completely diffused into TiC/Ti(CN) ceramic phase and Ni/Ni + Co binder phase, which is in agreement with previous studies [14,18]. The greatly expanded lattice parameters of each metal binder phase (see Table 4) correspond well with large amount of titanium, molybdenum, and tungsten contents found in the binder. From Table 6, it can be seen that the lattice parameter of Ti(CN) in cermet A and cermet B is less than standard TiC, while the lattice parameter of Ti(CN) in cermet C and cermet D is larger than standard Ti(CN). This observation suggests that TiC has been nitrided to form Ti(CN) in cermet A and cermet B, at the same time, the lattice parameters of cermet C and cermet D slightly expanded because some lattices of titanium in Ti(CN) have been occupied by molybdenum and tungsten.

The micrographs of cermet C and cermet D (see Fig. 2c and d) look unlike typical cermets microstructures. In addition to the classical core/rim structure (black core and grey rim), a new type of core/rim structure (white core and grey rim) appears. Since these images are obtained under SEM–BSE mode, the brighter color of white cores indicates that they must contain more heavy metallic elements than the rims. Subsequent SEM–EDX analysis confirmed this, which showed that the average white core metallic constitute is 61.5 at% Ti, 24.7 at% Mo, 13.8 at% W and 78.5 at% Ti, 7.9 at% Mo, 13.6 at% W for cermet C and cermet D, respectively, while their rim composition is the same as the rim surrounding black cores. Therefore, we can define this type of white core as (Ti, W, Mo) (C, N) heavy cores. A typical EDX spectrum of this heavy core phase is given in Fig. 4.

Since the raw materials are Ti(CN), WC and Mo not (Ti, W, Mo) (C, N) pre-alloyed carbides, these heavy cores must be formed during sintering stage. The exact formation mechanism of this kind of heavy core is still unknown, but might be reasonably speculated. Considering that the metallic constitute of heavy cores is similar to that of inner rims, their formation mechanisms should have something in common. Inner rim is widely believed to be formed during solid state sintering [7–9], and the heavy cores are also surrounded by grey rims that are formed after liquid phase appears. Based on these two facts, those heavy cores should be started to form at solid state sintering stage when open porosity still exists and the nitrogen activity is low. The formation process of heavy core can be described as follows: at solid state sintering stage, binder contains large amount of molybdenum and tungsten derived from solid dissolved WC and Mo_2C, at the same time, they precipitate on Ti(CN) particles just like inner rim. However, because of the extremely small particle size of Ti(CN) (from Fig. 1d, it can be seen that many Ti(CN) particle sizes are less than 100 nm), the diffusion length between Ti(CN) core and precipitated rim is significantly reduced. As a result, large amount of relatively small Ti(CN) cores are completely consumed by the growing inner rim (although the formation of heavy cores starts during solid state sintering, their growth and homogenization process carry on even after liquid phase appears) to present a core instead of a commonly observed rim morphology. Occasionally observed two-layered core/rim structure (very small Ti(CN) core surrounded by a thick inner and a thin outer rim) suggests that if this Ti(CN) core were a little bit smaller, it would be completely consumed to show a white core and grey rim structure too. As the sintering temperature further increases, liquid phase appears

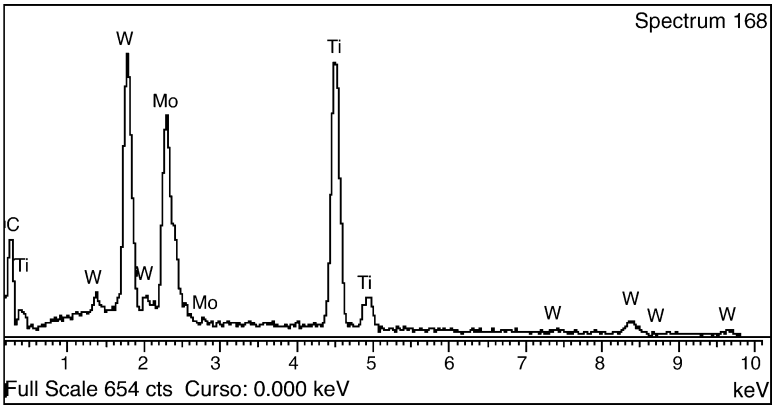

Fig. 4. A typical EDX spectrum of heavy cores.

and the outer rim forms on both heavy white cores and black Ti(CN) cores. Since a lot of titanium was found in heavy cores, a relatively low volume fraction of undissolved Ti(CN) cores found in cermet C and cermet D could be satisfactorily explained. However, it should be noted that the above discussion is only a preliminary attempt to investigate the formation mechanism of heavy cores based on limited information. Since using finer raw powder to manufacture cermet materials has become a trend, more research works should be done to further investigate this phenomenon.

Our previous research [19] has shown that molybdenum addition should be carefully chosen when designing cermet materials in order to optimize mechanical properties. Therefore, less molybdenum addition (5 wt%) was used in cermet D and its binder composition is a Ni + Co (50/50, wt%) mixture for a preliminary investigation of different binder phase's effects on ultrafine grade cermet materials.

These differences in raw material choosing make the microstructures of cermet C and cermet D differ considerably. As expected, the amount of molybdenum in each phase of cermet D is less than other cermet systems, especially in the outer rim. This phenomenon is understandable, for Mo_2C completely dissolved during solid state sintering [20], so large amount of them would have been consumed to form those heavy cores and less is left to form the outer rim. However, the tungsten content in each phase seems not to be influenced by different molybdenum additions. In cermet D, where molybdenum content is low, more titanium would be found while keeping tungsten atomic ratio relatively unchanged. Ti(CN) cores size was found to decrease with the increasing amount of molybdenum addition and this is consistent with literature [21]. More extremely small Ti(CN) cores are preserved in cermet C than in cermet D, which could be explained by two reasons: (1) The solubility of Ti(CN) in cobalt is higher than nickel. (2) Well-developed rim phase protects Ti(CN) cores from further dissolving at early stage.

Unfortunately, the microstructure of cermet C is rather inhomogeneous. The rim phase has connected to form continuous grey networks and the grain boundaries become unidentifiable. Moreover, much of the binder phase is trapped in isolated areas presenting grain-like shape which makes them sometimes hard to be distinguished from heavy cores. For above reasons, only black core size, black core volume fraction and rim phase volume fraction were measured in cermet C. The inhomogeneous microstructure should be inherited form the green compacts, that is, ball milling fails to fully homogenize various raw powders. The agglomeration of ultrafine Ti(CN) particles existed throughout the sintering stage and since its densification process carried out faster than other parts, it is hard for metal binder to infiltrate into the space between them and fill the porosity, which finally leads to not fully dense specimen. However, when half of nickel is replaced by cobalt as binders phase material, the agglomeration status of Ti(CN) cores and (Ti, Mo, W) (C, N) rims is greatly lessened, owing to better wettability of cobalt. In cermet D, intergranular-shaped binder phase can be easily identified. Here, the impact of cobalt on the microstructure and mechanical properties (will be discussed in Section 3.2) of ultrafine cermets is remarkable, so more systematic research works are needed to further investigate the role of cobalt as part of or complete binder phase material.

Table 7
Mechanical properties of each cermet system

Specimen	HV_{10} (kg/mm^2)	TRS (MPa)	K_{IC} (MPa $m^{1/2}$)	Density (g/cm^3)
A	1756 ± 52	1276 ± 71	9.2 ± 0.3	7.0695
B	1402 ± 46	1242 ± 57	12.3 ± 0.6	7.0957
C	1532 ± 66	1134 ± 48	7.6 ± 0.5	6.7642
D	1587 ± 39	1180 ± 30	10.3 ± 0.6	6.3916

3.2. Mechanical properties and discussion

Vickers hardness (HV_{10}), TRS, and the critical-stress intensity factor (K_{IC}) of each system were measured and the results are summarized in Table 7. Micrographs of fractured surfaces are given in Fig. 5. In general, all ultrafine grade cermets demonstrate enhanced hardness when compared with coarse cermet B, however, their TRS values are not as high as expected. Cermet B shows highest K_{IC} value.

By reducing the grain size from more than 2 μm to less than 500 nm, the hardness can be improved up to 25%. Besides of the well-established Hall–Petch hardening effect, another hardening source is the significantly reduced binder mean free path. According to the equation proposed in literature [22], cermet composite's hardness depends on a simple balance law, a combination of the hardness of various phases, and the metal binder hardness is in reverse proportion to binder mean free path. High volume fraction of undissolved Ti(CN) cores, the existence of Ni_2W_4C in the binder phase and ultrafine microstructure are possible explanations of the highest hardness achieved in cermet A. Although the total weight fraction of ceramic phase of cermet A and cermet C is the same (49 wt%), cermet C is softer than cermet A which could be explained by two reasons: (1) the hardness of TiN is lower than TiC [2] (we can assume $Ti(C_{0.5}N_{0.5})$ equals TiC+TiN, 50/50, at%); (2) the hardness of heavy core is lower than pure Ti(CN) core. In spite of obviously different morphology and raw material composition, the hardness values of cermet C and cermet D are very close. This result shows that hardness is not very sensitive to microstructure as strength and toughness do. More heavily solution hardened binder phase of cermet C demonstrated by its larger binder phase lattice parameter contributes more to its hardness, which makes its hardness only slightly lower than cermet D although its overall ceramic phase weight fraction is 10% less than cermet D.

Despite much finer microstructure, the brittle η phase reduces strength and toughness of cermet A, making them on

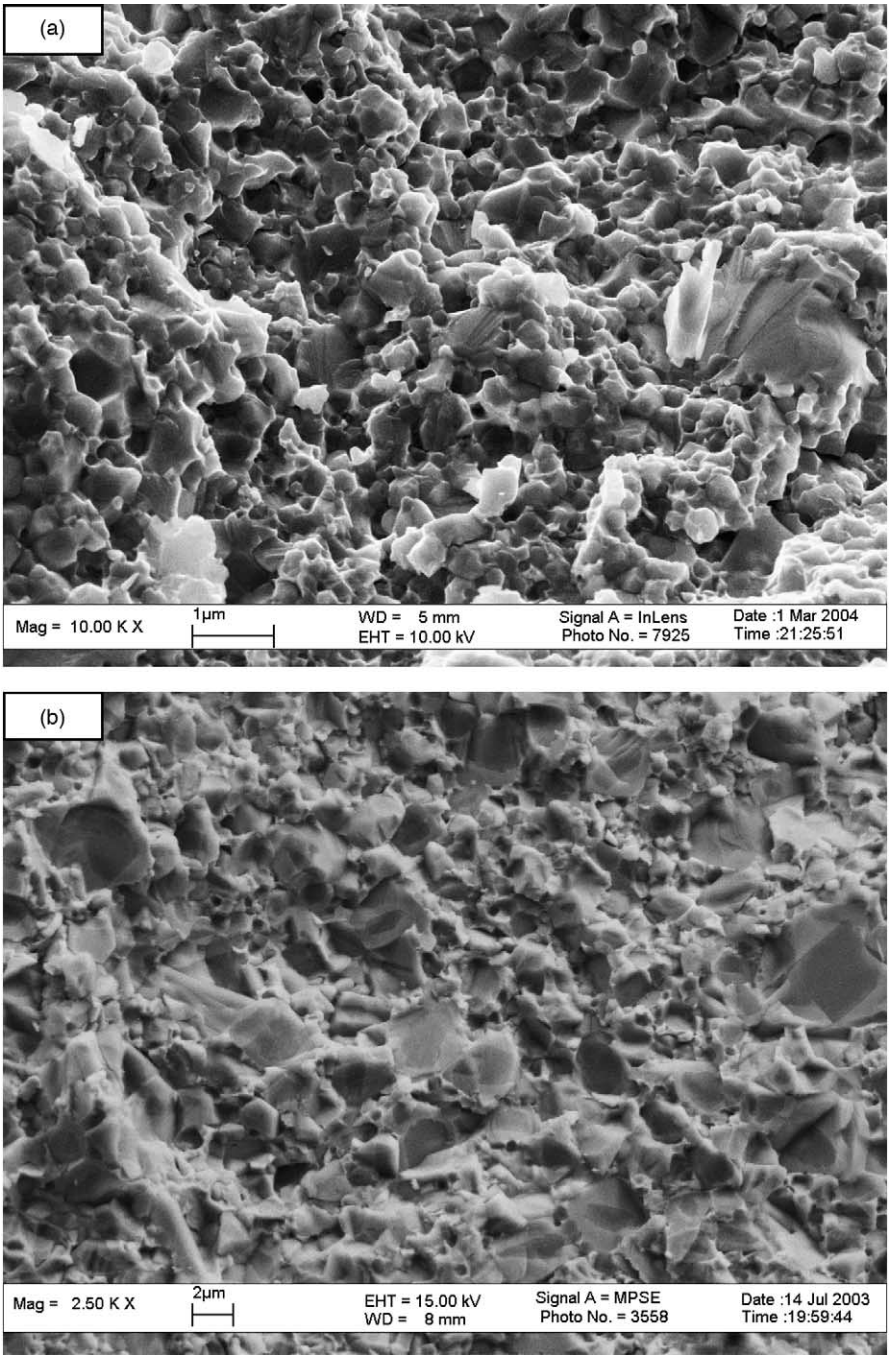

Fig. 5. SEM (SE) micrographs of fractured surface: (a) cermet A, (b) cermet B, (c) cermet C and (d) cermet D.

the same level as coarse cermet B. The presence of residual porosity (see Fig. 5c) should be responsible for the lowest strength and toughness found in cermet C, because to brittle-natured powder metallurgy materials, these pre-existed defects serve as fracture origins when loaded [23]. Cermet D benefits tremendously form its Ni + Co mixed binder composition, resulting in fully dense samples. In addition, the bond strength between binder and ceramic grains seems to be strengthened when cobalt is added, as it can been seen from Fig. 5d, in which transgranular fracture pattern can be clearly seen. Binder phase toughens cermets material by absorbing energy and relaxing stress through plastic deformation. So if the bond strength at binder/rim and rim/rim boundaries is strong, the crack-tip energy would dissipate during propagation [24]. Significantly, improved K_{IC} value in cermet D also demonstrates that better wetting condition enhances bond strength. However, the TRS values of cermet D is still lower than cermet A and cermet B, which may be attributed to its highest ceramic phase composition and high continuity of ceramic phase. Highest fracture

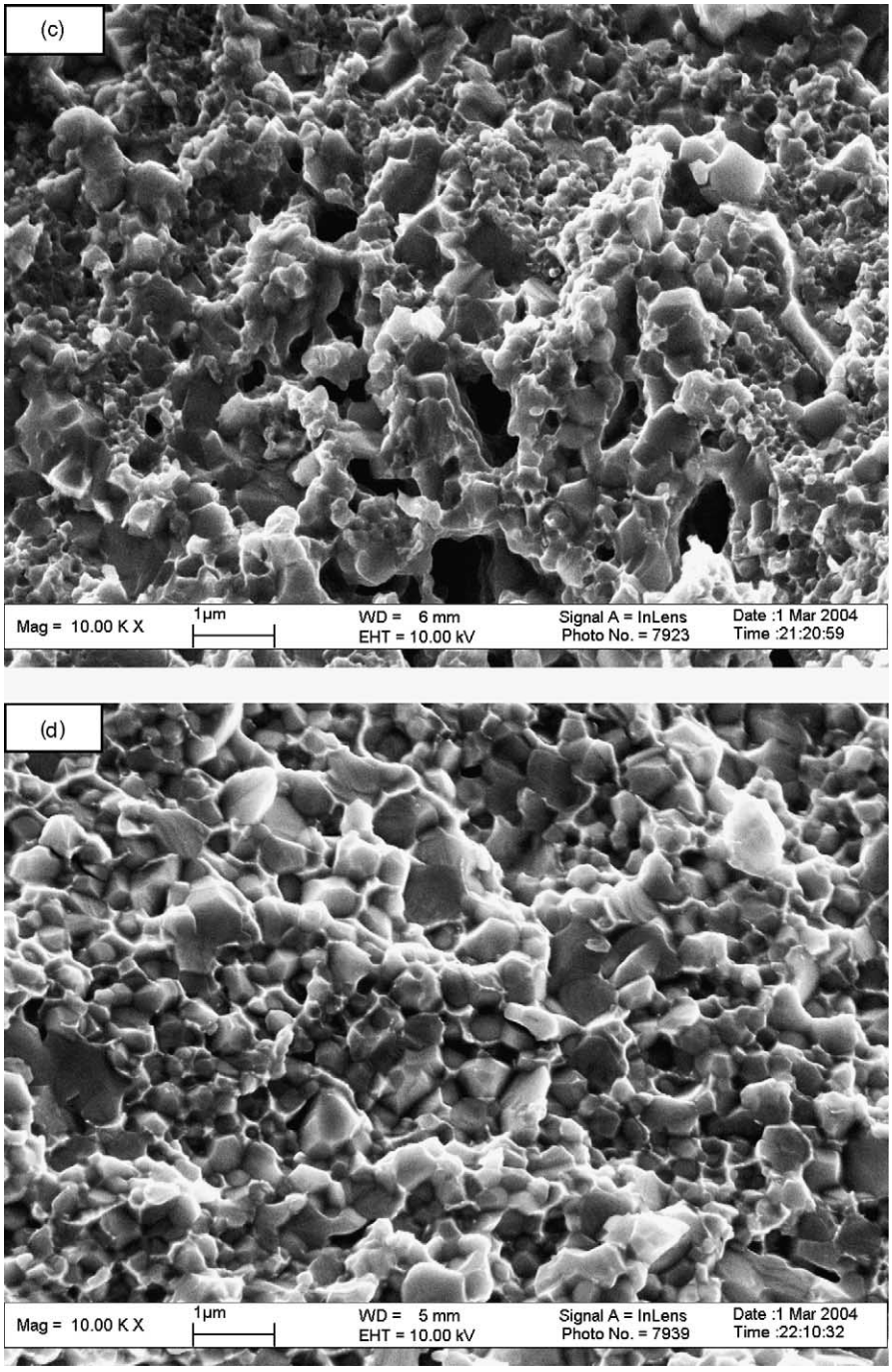

Fig. 5. (*Continued*).

toughness of cermet B is believed to be the result of combined effects: coarser carbonitride grains which promote crack curving and more properly distributed thicker binder phase which shields crack tip by plastic deformation.

4. Conclusion

In the present study, the microstructure and mechanical properties of various cermet systems fabricated from different raw materials and different initial particle size were investigated. The conclusion of this study can be summarized as follows:

(1) By using nano/submicron-sized starting powders, ultrafine grade cermets can be fabricated with little coarsing. The final grain size and phase volume fractions are greatly influenced by the dissolution behavior of various carbides in the binder phase during sintering.
(2) Initial powder particle size has a significant impact on the microstructure and properties of cermets. Because of

different particle size and size distribution, the extent of dissolution and reprecipitation differs greatly, resulting in different microstructural morphologies. η phase (Ni_2W_4C) was found in cermet A, as a result of decarbonization.

(3) A new type of core/rim structure (white core and grey rim) appears in cermets sintered from Ti(CN) initial powders, and the metallic constitute of this kind of heavy core is determined by SEM–EDX. According to their morphology and chemical composition, the formation mechanism of this phase is proposed.

(4) Using a Ni + Co (50/50, wt%) mixture as binder phase can significantly lessen the agglomeration status and make the microstructure more homogeneous. The reason of this phenomenon may owe to much better wettability of cobalt to Ti(CN).

(5) Although higher hardness is achieved in ultrafine grain cermets, their strength and toughness is not exciting. Much better overall properties can be expected if the amount of unwanted contaminates in raw materials could be reduced, the powder mixing work could be more properly done, and if the sintering conditions could be optimized.

Acknowledgements

Support for this work by Natural Science Foundation of China and Natural Science Foundation of Anhui Province under contract Nos. 50072003 and 03044902, respectively, are gratefully acknowledged.

References

[1] P. Ettmayer, W. Lengauer, The story of cermets, Powder Metall. Int. 2 (1989) 37–38.
[2] S. Zhang, Titanium carbonitride-based cermets: process and properties, Mater Sci. Eng. A163 (1993) 141–148.
[3] E.B. Clark, B. Roebuck, Extending the application areas for titanium carbonitride cermets, Refract. Met. Hard Mater. 11 (1992) 23–27.
[4] G.E. D'Errico, S. Bugliosi, E. Guglielmi, Tool-life reliability of cermet inserts in milling tests, J. Mater. Proc. Technol. 77 (1998) 337–343.
[5] T. Cutar, T. Viatte, G. Feusier, W. Benoit, Microstructure and high temperature mechanical properties of $TiC_{0.7}N_{0.3}$–Mo_2C–Ni cermets, Mater. Sci. Eng. A209 (1996) 218–227.
[6] S. Kang, Stability of Ni in Ti(CN) solid solutions for cermet applications, Powder Metall. 40 (1997) 139–142.
[7] S.-Y. Ahn, S.-W. Kim, S. Kang, Microstructure of Ti(CN)–WC–NbC–Ni cermets, J. Am. Ceram. Soc. 84 (4) (2001) 843–849.
[8] S.Y. Ahn, S. Kang, Formation of core/rim structure in Ti(C, N)–WC–Ni cermets via a dissolution and precipitation process, J. Am. Ceram. Soc. 83 (6) (2000) 1489–1494.
[9] P. Lindahl, A.E. Rosén, P. Gustafson, U. Rolander, H.O. Andrén, Effect of pre-alloyed raw materials on the microstructure of a (Ti,W)(C, N)–Co cermet, Int. J. Refract. Met. Hard Mater. 18 (2000) 273–279.
[10] K. Jia, T.E. Fischer, B. Gallois, Microsturcture, hardness and toughness of nanostructured and conventional WC–Co composites, Nanostruct. Mater. 10 (5) (1998) 875–891.
[11] N. Liu, Y.D. Xu, H. Li, G.H. Li, L.D. Zhang, Effect of nano–micro TiN addition on the microstructure and mechanical properties of TiC based cermets, J. Eur. Ceram. Soc. 22 (2002) 2409–2414.
[12] L.V. Azaroff, M.J. Buerger, The Powder Method, McGraw-Hill, New York, 1958.
[13] P. Lindahl, T. Mainert, H. Jonsson, H.-O. Andrén, Microstructure and mechanical properties of a (Ti, W, Ta, Mo)(C, N)-(Co, Ni)-type cermet, J. Hard Mater. 4 (1993) 187–204.
[14] P. Lindahl, P. Gustafson, U. Rolander, L. Stals, H.-O. Andrén, Microstructure of model cermets with high Mo or W content, Int. J. Refract. Met. Hard Mater. 17 (1999) 411–421.
[15] H. Yoshimura, T. Sugisawa, K. Nishigaki, H. Doi, Reaction during sintering and the characteristics of TiC–20TiN–15WC–10TaC–9Mo–5.5Ni–11Co cermet, Int. J. Refract. Met. Hard Mater. 12 (1983) 170–174.
[16] F. Qi, S. Kang, A study on microstructural changes in Ti(CN)–NbC–Ni cermets, Mater Sci. Eng. A251 (1998) 276–285.
[17] J. Zackrisson, H.-O. Andrén, Effect of carbon content on the microstructure and mechanical properties of (Ti, W, Ta, Mo) (C, N) cermets, Int. J. Refract. Met. Hard Mater. 17 (1999) 265–273.
[18] J.K. Yang, H.-C. Lee, Microstructural evolution during the sintering of a Ti(C, N)–Mo2C–Ni alloy, Mater Sci. Eng. A209 (1996) 213–217.
[19] N. Liu, Y. Xu, Z. Li, M. Chen, G. Li, L. Zhang, Influence of molybdenum addition on the microstructure and mechanical properties of TiC-based cermets with nano-TiN modification, Ceram. Int. 29 (2003) 919–925.
[20] H-O. Andrén, U. Rolander, P.S. Lindahl, Phase composition in cemented carbides and cermets, Int. J. Refract. Met. Hard Mater. 12 (1993–1994) 107–113.
[21] D. Mari, S. Bolognini, G. Feusier, T. Cutard, C. Verdon, T. Viatte, W. Benoit, TiMoCN based cermets. Part I. Morphology and phase composition, Int. J. Refract. Met. Hard Mater. 21 (2003) 37–46.
[22] D. Mari, S. Bolognini, G. Feusier, T. Cutard, T. Viatte, W. Benoit, TiMoCN based cermets. Part II. Microstructure and room temperature mechanical properties, Int. J. Refract. Met. Hard Mater. 21 (2003) 47–53.
[23] M. Ueki, T. Saito, H. Suzuki, The sinterability of nitrogen containing TiC–Mo2C–Ni cermet, J. Jpn. Soc. Powder Powder Metall. 36 (4) (1989) 371–373.
[24] A. Bellosi, V. Medri, F. Monteverde, Processing and properties of Ti(C, N)–WC-based materials, J. Am. Ceram. Soc. 84 (11) (2001) 2669–2676.